



Lung microhaemorrhage drives oxidative/inflammatory damage in α_1 -antitrypsin deficiency

Cesare Saltini^{1,9}, Naweed Mohammad^{1,9}, Yan Xin², Rodolfo Alvarado³, Andrew J. Ghio⁴, Craig G. Money Penny¹, Alberto Riva⁵, Dongtao Fu⁶, Tammy Flagg¹, Giovanni F.A. Saltini¹, Ivan Arisi⁷, Kristianna M. Fredenburg⁶, Yang Zhang⁸, Jorge E. Lascano¹ and Mark Brantly¹

¹Division of Pulmonary, Critical Care and Sleep Medicine, College of Medicine, University of Florida, Gainesville, FL, USA. ²National High Magnetic Field Laboratory, Florida State University, Tallahassee, FL, USA. ³Interdisciplinary Center for Biotechnology Research, Electron Microscopy Core, University of Florida, Gainesville, FL, USA. ⁴United States Environmental Protection Agency, Chapel Hill, NC, USA. ⁵Interdisciplinary Center for Biotechnology Research, Bioinformatics Core, University of Florida, Gainesville, FL, USA. ⁶Department of Pathology, Immunology, and Laboratory Medicine, University of Florida, Gainesville, FL, USA. ⁷Bioinformatics Facility, European Brain Research Institute, Rome, Italy. ⁸Department of Medicine, University of Florida, Gainesville, FL, USA. ⁹These authors contributed equally.

Corresponding author: Cesare Saltini (Cesare.Saltini@medicine.ufl.edu)



Shareable abstract (@ERSpublications)

BAL and tissue markers show evidence of recurrent alveolar haemorrhage in α_1 -antitrypsin-deficient subjects, likely driven by unopposed neutrophil elastase, causing the release of free haem, and subsequent pro-inflammatory activation and oxidative damage <https://bit.ly/3lg8K8Y>

Cite this article as: Saltini C, Mohammad N, Xin Y, *et al.* Lung microhaemorrhage drives oxidative/inflammatory damage in α_1 -antitrypsin deficiency. *ERJ Open Res* 2023; 0: 00662-2022 [DOI: 10.1183/23120541.00662-2022].

Copyright ©The authors 2023

This version is distributed under the terms of the Creative Commons Attribution Non-Commercial Licence 4.0. For commercial reproduction rights and permissions contact permissions@ersnet.org

Received: 30 Nov 2022
Accepted: 07 March 2023

Abstract

Background Animal models using intratracheal instillation show that elastase, unopposed by α_1 -antitrypsin (AAT), causes alveolar damage and haemorrhage associated with emphysematous changes. The aim of the present study was to characterise any relationship between alveolar haemorrhage and human AAT deficiency (AATD) using bronchoalveolar lavage (BAL) and lung explant samples from AATD subjects.

Methods BAL samples (17 patients, 15 controls) were evaluated for free haem (iron protoporphyrin IX) and total iron concentrations. Alveolar macrophage activation patterns were assessed using RNA sequencing and validated *in vitro* using haem-stimulated, monocyte-derived macrophages. Lung explants (seven patients, four controls) were assessed for iron sequestration protein expression patterns using Prussian blue stain and ferritin immunohistochemistry, as well as ferritin iron imaging and elemental analysis by transmission electron microscopy. Tissue oxidative damage was assessed using 8-hydroxy-2'-deoxyguanosine immunohistochemistry.

Results BAL collected from AATD patients showed significantly elevated free haem and total iron concentrations. Alveolar and interstitial macrophages in AATD explants showed elevated iron and ferritin accumulation in large lysosomes packed by iron oxide cores with degraded ferritin protein cages. BAL macrophage RNA sequencing showed innate pro-inflammatory activation, replicated *in vitro* by haemin exposure, which also triggered reactive oxygen species generation. AATD explants showed massive oxidative DNA damage in both lung epithelial cells and macrophages.

Conclusions BAL and tissue markers of alveolar haemorrhage, together with molecular and cellular evidence of macrophage innate pro-inflammatory activation and oxidative damage, are consistent with free haem stimulation. Overall, this initial study provides evidence for a pathogenetic role of elastase-induced alveolar haemorrhage in AATD emphysema.

Introduction

SERPINA1 gene “null” or “deficient” mutations can cause defective or absent production of α_1 -antitrypsin (AAT), the serine protease inhibitor that irreversibly binds and inactivates neutrophil elastase [1]. These mutations are associated with lung injury, including early-onset emphysema [2]. The role of the loss of AAT anti-elastase capacity in AATD-associated emphysema was demonstrated in animal models of intratracheal elastase instillation, where emphysema was prevented by co-instillation of human serum, but not AATD subjects' serum. In these studies, elastase-induced elastin and whole alveolar wall damage were



associated with erythrocyte influx into alveolar spaces [3], haemoglobin release/degradation [4] and macrophage pro-inflammatory activation [5, 6], with iron accumulation and reactive oxygen species (ROS) generation in alveolar macrophages and epithelial cells [7]. Thus, this investigation suggested that alveolar bleeding occurs in AATD subsequent to elevated unopposed elastase.

In acute lung injury models, alveolar inflammation can be associated with microhaemorrhage, intra-alveolar haemolysis and liberation of haem [8]. This can then lead to abnormal levels of free haem in alveolar fluids and iron accumulation in lung macrophages, which can both function as markers of alveolar haemorrhage [9]. Extravasated red blood cells, free haem and iron can trigger the generation of ROS and drive macrophages to a pro-inflammatory state [10–12] that has been characterised as an M1-like pro-inflammatory phenotype [13–15].

This study evaluated bronchoalveolar lavage (BAL) levels of free haem, BAL iron levels, BAL macrophage iron accumulation and BAL macrophage activation in AATD-affected and control subjects, in order to acquire *ex vivo* evidence of alveolar microhaemorrhage in AATD and associated damaging effects.

Methods

Study populations

Tissue samples (table 1) were obtained from AATD lung explants (n=7, pulmonary division tissue bank IRB201501133) from unaffected lungs (n=4; University of Florida Clinical and Translational Science Institute IRB201701597). The control and AATD-affected subjects undergoing bronchoscopy with lavage differed, to some extent, in age and smoking history (table 1).

Unused BAL aliquots were obtained from AATD individuals (n=17) enrolled in a clinical study (IRB20140928) [16]. None of the AATD subjects was on AAT augmentation therapy for 6 weeks preceding the procedure. BAL samples were also obtained from healthy individuals after informed consent (n=6 (University of Florida IRB201501133); n=9 (University of North Carolina IRB91–0679)) (table 1).

Peripheral blood mononuclear cells were obtained from AATD individuals (n=4) and healthy individuals (n=4) (University of Florida IRB2015-01051).

BAL

BAL was carried out as described previously [17]. The lavage fluid recovered was stored on ice to be processed within 3 h. Cytopreps were stained using Diff-Quik and Prussian blue. BAL alveolar

TABLE 1 Study populations for bronchoalveolar lavage (BAL) and tissue analysis

	Control	AATD
BAL population		
Subjects	15	17
Female/male	3/12	13/4
Age (years)	31.1±11.4	57.2±7.8*
Smoking history (pack-years)	0.0±0.0 [#]	1.4±0.9 [¶]
FEV ₁ (%)	111.7±13.7	80.1±18.2**
Macrophages (%)	87.7±3.8	70.5±24.0**
Neutrophils (%)	1.5±1.1	23.7±24.3***
NE (nM)	4.6±4.8 [#]	307.3±350.8**
AAT (nM)	2480.0±466.8 [#]	256.3±185.0***
Haemopexin (µM)	4.9±5.2 [#]	2.6±1.9 [¶]
IL-6 (pg·mL ⁻¹)	158.2±179.8 [#]	1300.4±1418.7**
IL-8 (pg·mL ⁻¹)	1421.1±957.1 [#]	7773.3±11 089.3*
Tissue explant population		
Subjects (n)	4	7
Female/male	3/1	2/5
Age (years)	65.3±10.7	56.1±6.5 [¶]
Smoking history (pack-years)	25.3±21.6	26.6±27.2 [¶]
Data are presented as n or mean±SD, unless otherwise stated. AATD: α ₁ -antitrypsin deficiency; FEV ₁ : forced expiratory volume in 1 s; NE: neutrophil elastase; AAT: α ₁ -antitrypsin; IL: interleukin. [#] : data not available for all 15 control BAL subjects; [¶] : nonsignificant. *: p<0.05; **: p<0.01; ***: p<0.001.		

macrophages (AlvMacs) were isolated by adherence to tissue culture plates (serum-free medium, 37°C, 60 min). Due to BAL fluid availability limitations, total protein concentration was not measured. BAL urea levels were measured to determine epithelial lining fluid (ELF) dilution, hence the normalised concentration of cellular and molecular component of BAL, as described previously [17]. Such use of urea has been recommended by previous investigation in humans as well as in animals (supplementary methods).

BAL free haem (iron protoporphyrin IX) was measured using the Hemin Assay Kit and the QuantiChrom Heme Assay Kit (measuring haem + nonencapsulated haemoglobin); haemopexin using an ELISA kit; and ferritin and transferrin using ELISA kits. Interleukin (IL)-6 and IL-8 were measured using ELISA, and AAT and neutrophil elastase using ELISA, as described in [16]. BAL non-haem iron and total iron concentration were measured using inductively coupled plasma optical emission spectroscopy operated at a wavelength of 238.204 nm.

Microscopy

Formalin-fixed paraffin-embedded (FFPE) tissue sections (4 µm) were stained with haematoxylin and eosin and Prussian blue stain. Immunohistochemistry was carried out using ferritin light chain, ferritin heavy chain and 8-hydroxy-2'-deoxyguanosine (8-OHdG). Staining intensity was quantified by acquiring the complete tissue section images using a Keyence BZ-X710 microscope and analysed using ImageJ.

Bright-field (BF) transmission electron microscopy (TEM) was carried out on AATD (n=3) and control FFPE blocks (n=2) by punching out areas of interest, identified on Prussian blue-stained slides (supplementary figure S1a) and processing for TEM analysis. Although fixation and embedding prevented cytoplasmic structure visualisation, iron was imaged with high accuracy (supplementary figure S1a-d).

High-angle annular dark-field scanning transmission electron microscopy (HAADF-STEM) imaging and elemental analysis were performed, and the measurement of ferritin loading numbers in vesicles was carried out.

RNA sequencing

Differential gene expression (DGE) analysis was carried out on isolated BAL macrophages by total RNA sequencing. Sequences were deposited to the National Center for Biotechnology Information Gene Expression Omnibus (GEO) repository (GEO accession number GSE194313).

Multidimensional scaling separated control (n=6) from AATD (n=6) samples and identified two AATD subgroups (n=3 each; supplementary figure S3a). Further analysis was carried out utilising the full AATD2 DGE dataset with nine gene sets identifying macrophage activation patterns [18].

In vitro studies

Monocytes from AATD and control leukapheresis samples were cultured as described previously [19] to generate monocyte-derived macrophages (MDMs). The expression of genes characterising iron sequestration protein expression patterns (haem oxygenase 1 (HMOX1), Spi-C transcription factor (SPIC) and solute carrier family 40 member 1/ferroportin 1 (SLC40A1/FPN)) [20] was assessed using reverse transcriptase (RT) quantitative (q)PCR in haemin-stimulated MDMs. To model haem-induced AlvMac activation, MDMs were exposed to haemin concentrations (2.5 and 10 µM, serum-free medium, 3 h) as described by FIGUEIREDO *et al.* [11]. ROS generation was measured fluorometrically, using CM-H2DCFDA (dichlorodihydrofluorescein diacetate). AAT inhibitory capacity of haem-induced MDM ROS generation was tested using human AAT at normal alveolar fluid concentration (3 µM).

RT-qPCR was used as described previously [19] to quantify expression of pro-inflammatory factors associated with the macrophage pattern induced by TPP [18] designated as M-TPP. These factors include IL-1, tumour necrosis factor (TNF), IL-6, C-X-C motif chemokine ligand (CXCL)8, prostaglandin-endoperoxide synthase (PTGS)2, X-box binding protein (XBP)1 and XBP1 spliced, and the M1 chemokines CXCL9, CXCL10 and CXCL11.

Statistical methods

Study population, microscopy and *in vitro* study data are expressed as mean±SD or percentage, as appropriate. Comparisons between groups were made by using the two-sample t-test. The paired t-test was used for the analysis of different transcript isoforms. A p-value <0.05 was considered significant.

Supplementary methods

Further details on BAL, histochemistry, electron microscopy, RNA sequencing, *in vitro* haem exposure and statistical methods are provided in the supplementary methods.

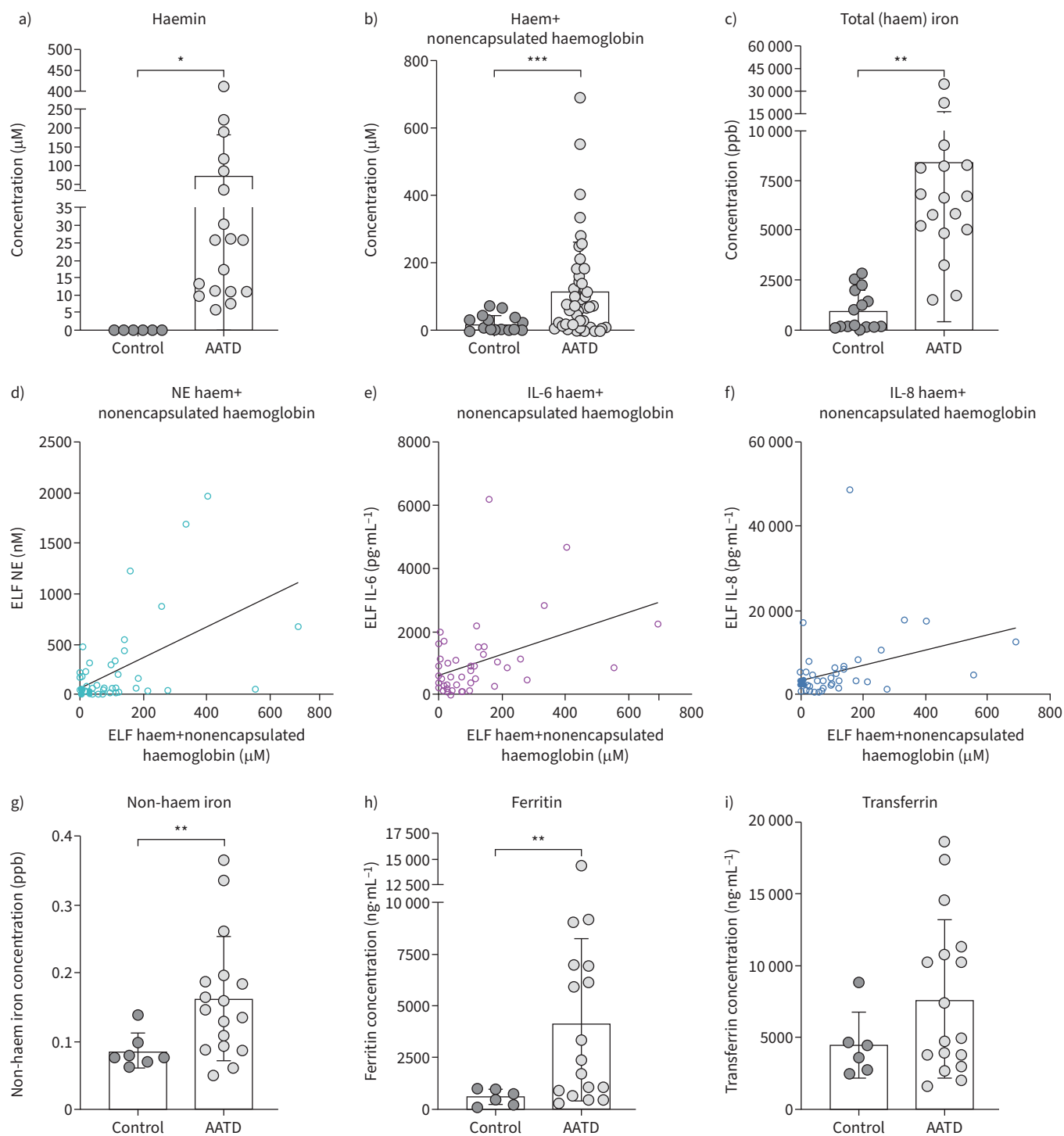


FIGURE 1 Epithelial lining fluid (ELF) levels of **a**) haemin (control $0.2 \pm 0.1 \mu\text{M}$, α_1 -antitrypsin deficiency (AATD) $72.0 \pm 108.7 \mu\text{M}$; $p=0.0149$) and **b**) haem+nonencapsulated haemoglobin (control $21.5 \pm 25.0 \mu\text{M}$, AATD $115.0 \pm 144.5 \mu\text{M}$; $p=0.00004$). **c**) Total (haem) iron ELF levels are shown as inductively coupled plasma optical emission spectroscopy (ICPOES) total (non-haem and haem) iron (control $970.9 \pm 1015.1 \text{ ppb}$, AATD $8412.5 \pm 7997.5 \text{ ppb}$; $p=0.0015$). Haem+nonencapsulated haemoglobin was correlated with **d**) neutrophil elastase (NE), **e**) interleukin (IL)-6 and **f**) IL-8 (Pearson coefficient $r=0.516$, $p=0.0002$ and Spearman coefficient $r_s=0.397$, $p=0.005$, $r=0.408$, $p=0.004$; and $r_s=0.320$, $p=0.028$, $r=0.330$, $p=0.022$ and $r_s=0.373$, $p=0.009$, respectively). ELF iron levels are shown as **g**) ICPOES non-haem iron (control $0.086 \pm 0.025 \text{ ppb}$, AATD $0.162 \pm 0.090 \text{ ppb}$; $p=0.0043$); and as **h**) ferritin (control $563.8 \pm 373.2 \text{ ng}\cdot\text{mL}^{-1}$, AATD $4162.4 \pm 4112.3 \text{ ng}\cdot\text{mL}^{-1}$; $p=0.0024$) and **i**) transferrin (control $4458.7 \pm 2283.6 \text{ ng}\cdot\text{mL}^{-1}$, AATD $7669.2 \pm 5464.7 \text{ ng}\cdot\text{mL}^{-1}$; $p=0.0614$) protein concentrations. Data are shown as ELF concentrations, normalised to bronchoalveolar lavage fluid urea concentrations, as described previously [17]. *: $p<0.05$; **: $p<0.01$; ***: $p<0.001$ (t-test).

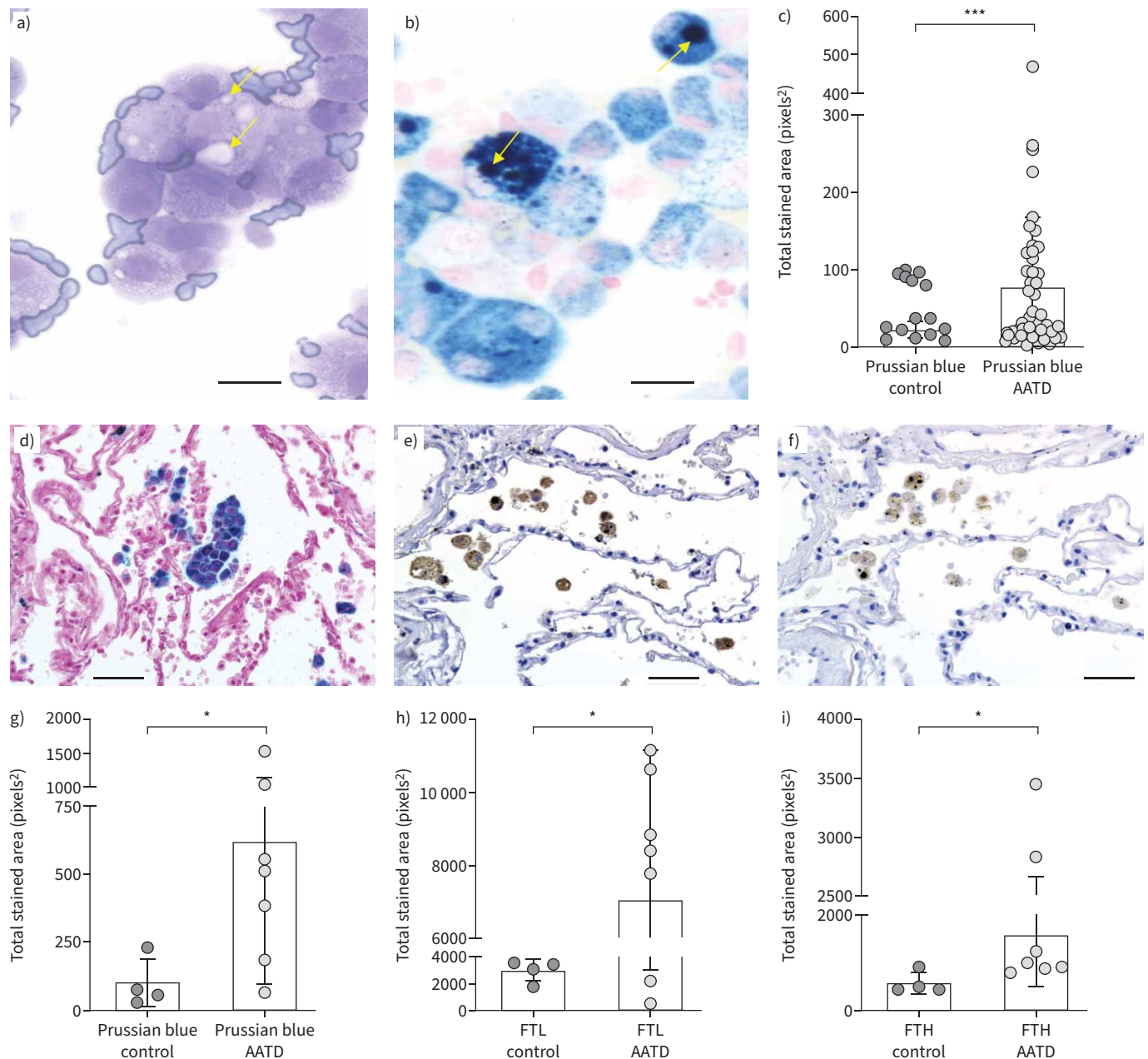


FIGURE 2 a) Diff-Quik stained cytopreps of α_1 -antitrypsin deficiency (AATD) bronchoalveolar lavage cells show alveolar macrophages, with numerous adherent red blood cells and erythrophagocytic figures; b) Prussian Blue stained cytopreps demonstrate significantly greater iron accumulation in AATD macrophages (control 24.4 ± 12.4 pixels², AATD 75.6 ± 90.8 pixels²; $p=0.00015$) c) compared to control. Arrows indicate examples of erythrocyte-like inclusions in a) and areas of iron accumulation in b). Scale bars= $20 \mu\text{m}$. d) Prussian blue iron stain, e) ferritin light chain (FTL) and f) ferritin heavy chain (FTH) in AATD lung explanted tissue. Scale bars= $50 \mu\text{m}$. ImageJ quantitation of staining intensity for g) Prussian blue (control 99.0 ± 88.5 pixels², AATD 615.5 ± 521.1 pixels²; $p=0.020$), h) FTL (control 2949.0 ± 775.4 pixels², AATD 7079.7 ± 4111.2 pixels²; $p=0.019$) and i) FTH (control 575.6 ± 228.6 pixels², AATD 1584.2 ± 1085.5 pixels²; $p=0.025$); all significantly higher in AATD compared to controls. *: $p<0.05$; ***: $p<0.001$ (t-test).

Results

BAL markers of alveolar haemorrhage

The control and AATD-affected subjects undergoing bronchoscopy with lavage differed in age and smoking history (table 1). BAL levels of free haem were significantly elevated in AATD subjects compared to controls (figure 1a, b), indicating recent alveolar microhaemorrhage. Consistent with haem levels, total iron concentration in the BAL was significantly elevated in AATD subjects (figure 1c). Haem

(measured as haem+nonencapsulated haemoglobin) in BAL fluids collected from the right upper, right middle and lingular lobes of AATD subjects (n=47 samples) showed different levels, suggesting localised rather than diffuse haemorrhage.

Compared to controls, AATD subjects had significantly higher BAL levels of neutrophil elastase, IL-6 and IL-8 (table 1). Concentrations of neutrophil elastase, IL-6 and IL-8 in the BAL correlated with haem levels (figure 1d–f). Neutrophil numbers, although significantly elevated in the BAL from AATD subjects (table 1), did not correlate to haem levels. Haemopexin levels in AATD (table 1) were >27.7 times lower than haem on a molar basis. Accordingly, the haemopexin concentrations were considered insufficient to bind and transfer the haem to catabolising cells [12], comparable to levels of AAT [21]. BAL levels of non-haem iron and ferritin were significantly higher in AATD than control subjects, while transferrin was not (figure 1g–i). BAL cytopreps from AATD subjects showed alveolar macrophages with adherent red blood cells or phagocytosed erythrocyte-like inclusions, and intracellular accumulation of haemosiderin (figure 2a, b). Prussian blue stain intensity was significantly higher in those AlvMacs collected from AATD subjects relative to controls (figure 2c).

Prussian blue stain and ferritin immunohistochemistry intensity on AATD lung sections showed significantly higher intensities than control samples (figure 2d and g, e and h, f and i), indicating iron accumulation in alveolar and interstitial macrophages [9].

Electron microscopy assessment of macrophage iron accumulation pattern

AlvMacs collected from control subjects showed isolated ferritin iron cores in the cytoplasm and lysosome-like vesicles (figure 3a and b), with no prominent lysosomal accumulation observed in the interstitial macrophages (figure 3c and d). In contrast, AATD AlvMacs showed numerous, large lysosomal vesicles densely packed with iron cores (figure 3e and f). Together with these metal-replete lysosomal vesicles, AlvMacs showed larger phagolysosomal vesicles containing nonferrous material with an iron-containing peripheral layer (supplementary figure S1e–h). Interstitial macrophages contained similar iron-packed lysosomal vesicles (figure 3g and h). Altered interstitial capillary vessels, engorged with red blood cells seeping into alveolar spaces, were also observed (supplementary figure S1c and g).

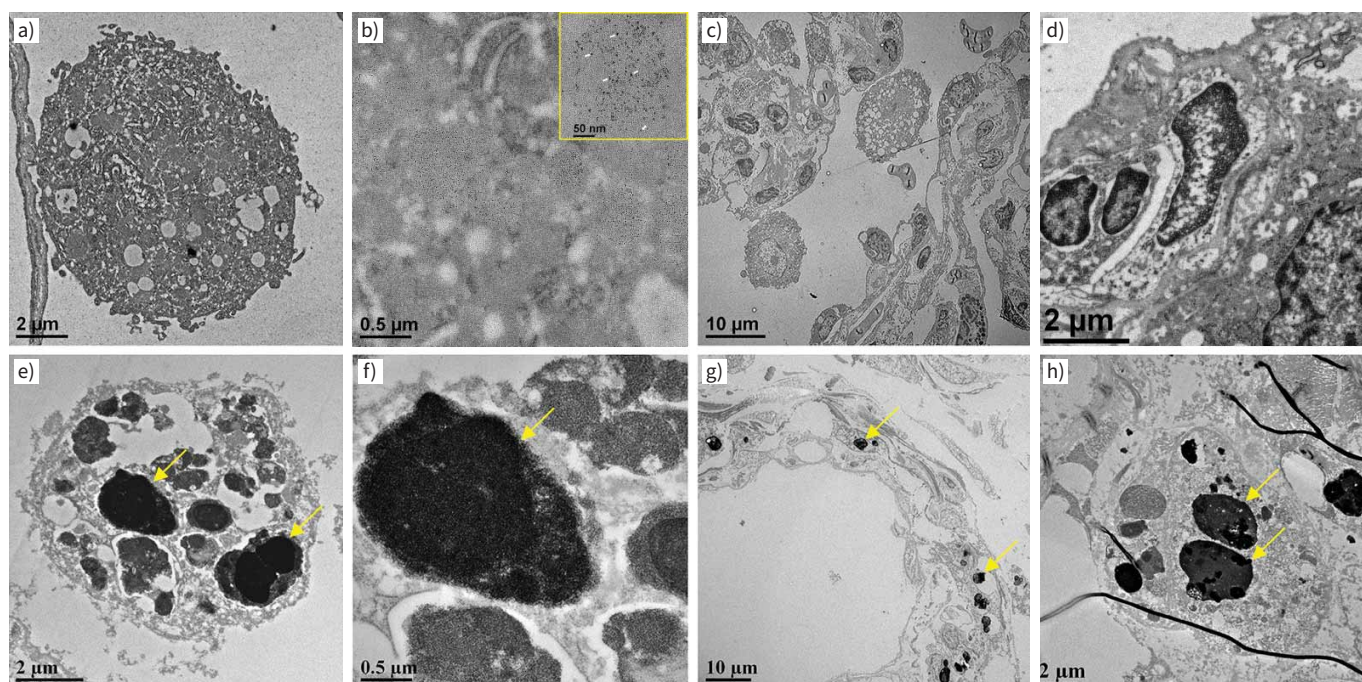


FIGURE 3 a) Control alveolar macrophages (AlvMacs) contain possibly numerous vesicles or remnants of lipid bodies; b) at higher magnification (inset), ferritin cores appear dispersed throughout the cytoplasm. AlvMacs seen between c) alveolar walls and d) alveolar interstitial cells did not show iron core accumulation. e, f) α_1 -Antitrypsin deficiency AlvMacs are characterised by numerous, densely iron-repleted lysosomal vesicles (arrows). g, h) Lysosomal and phagolysosomal content are seen similarly in interstitial macrophages (arrows).

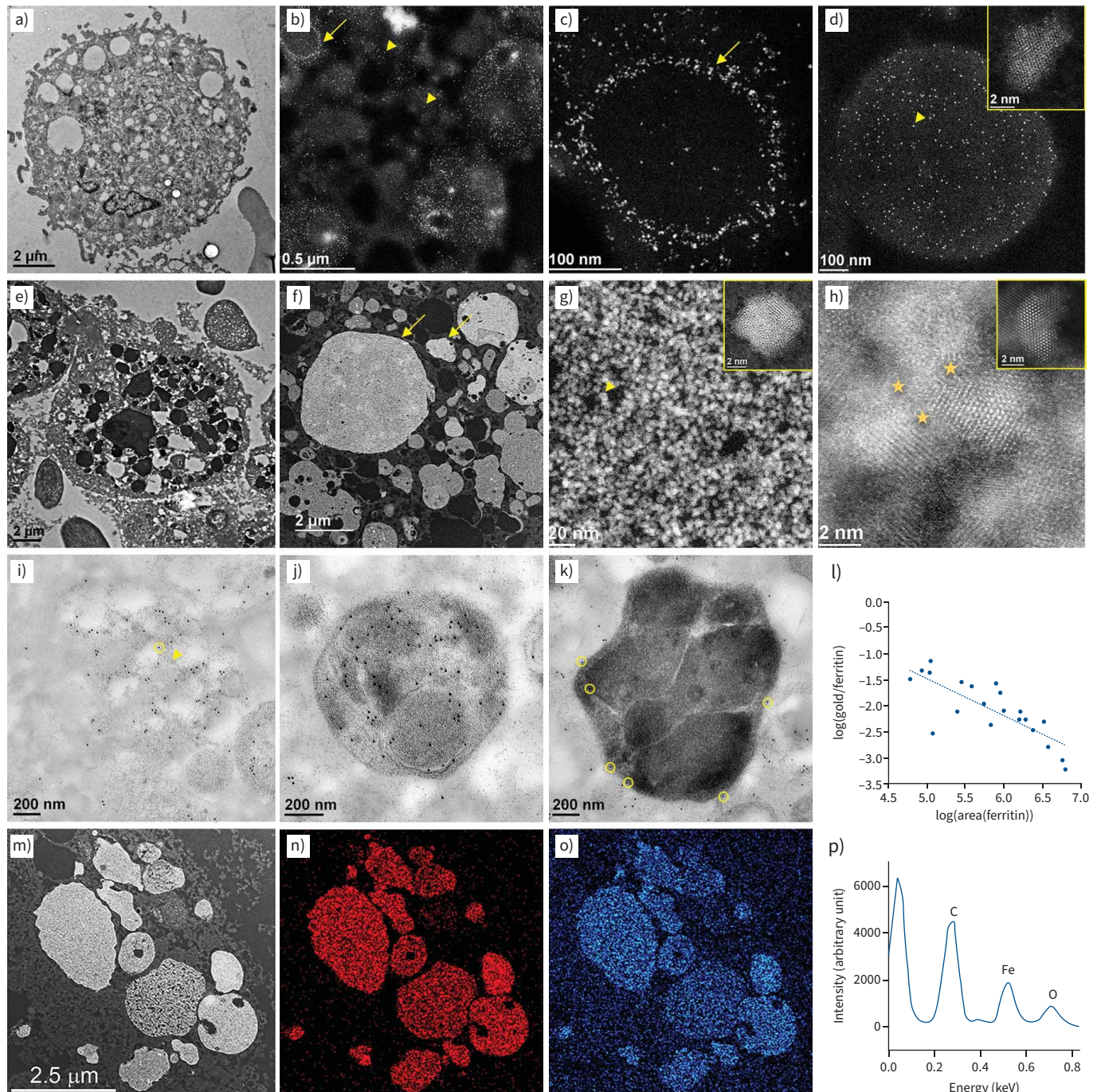


FIGURE 4 Control alveolar macrophages (AlvMacs) (a, bright-field transmission electron microscopy (BF-TEM)) contain loosely packed ferritin cores in the cytoplasm (b, d, arrowheads) and/or arranged at the periphery of lysosomes/vesicles (b, c, arrows) by high-angle annular dark-field scanning transmission electron microscopy (HAADF-STEM) imaging (b–d). At atomic resolution, where the bright dots represent single iron atoms of a ferritin core (d, inset), control AlvMac ferritins are characterised as partially loaded with iron and have a crystalline structure of ferrihydrite. α_1 -Antitrypsin deficiency (AATD) AlvMacs (e, BF-TEM) contain large lysosomal vesicles (f–h, HAADF-STEM) repleted with iron at varying densities (f, arrows). In g) densely packed ferritin core vesicles (arrowhead), ferritin cores appear to be fully loaded with iron (inset) and show h) the oxidised crystalline structure of haematite α -Fe₂O₃ (inset). Most AATD AlvMac ferritins packed in lysosomal and phagolysosomal vesicles lack the 1–2-nm halo representing their protein cages (h, stars). The absence of the ferritin protein cage suggests ferritin degradation, as seen in haemosiderin. Immunoelectron microscopy assessment of ferritin light chain (FTL) expression in AATD AlvMacs. Ferritin iron cores (8 nm dense particles, arrowhead) and FTL antibody-bound with colloidal gold particles (12 nm dense particles, circles) are shown in the i) cytoplasm, j) lysosome and k) densely repleted phagolysosomes. The negative correlation between ferritin iron cores and FTL immunogold binding, indicating the presence of undegraded FTL protein, suggests ferritin protein cage degradation in denser lysosomes (l) (Pearson coefficient $r = -0.79$, $p = 0.000034$). m) Elemental mapping and spectrometry validate iron density of AlvMac lysosomes as assessed by HAADF-STEM analysis. Energy-dispersive X-ray spectroscopy (EDS) maps show n) iron and o) oxygen in lysosomes, with p) individual lysosomes loaded with iron confirmed by EDS.

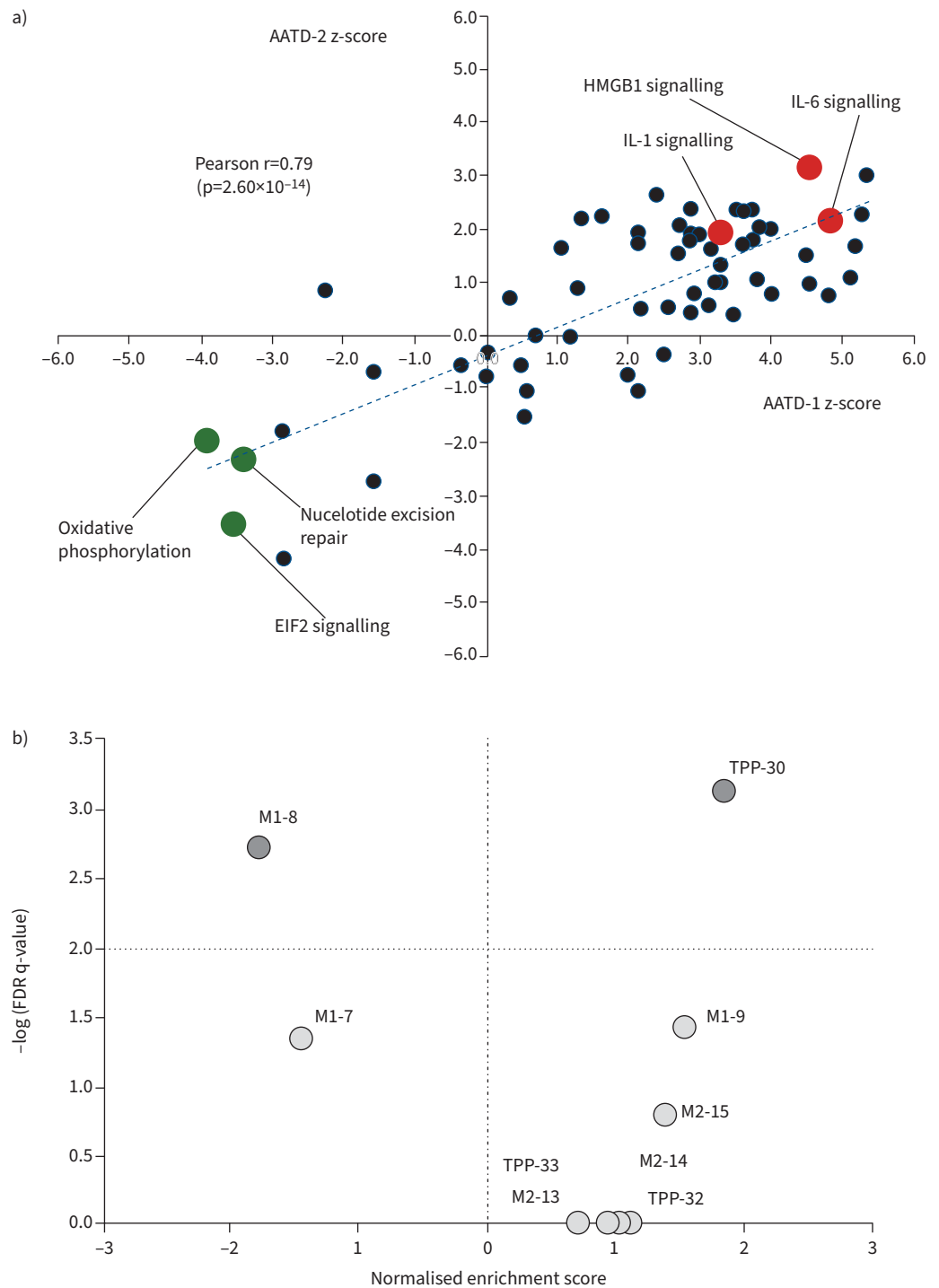


FIGURE 5 a) Scatter plot of the z-scores for the significantly enriched canonical pathways (α_1 -antitrypsin deficiency (AATD) versus AATD2). The most significantly activated pathways are highlighted red (positively enriched) or green (negatively enriched). b) Gene set enrichment analysis of the AATD2 full differential gene expression dataset with nine gene sets representing classic activation patterns M1 and M2, and the TPP gene lists of innate immune activation patterns [18]. The volcano plot shows positive (TPP-30, activated by tumour necrosis factor, PGE2 and P3C) and negative (M1-8, activated by interferon- γ) enrichment. The full list of gene sets is shown in supplementary table S1, sheet 1. HMGB1: high mobility group box 1; IL: interleukin; EIF2: eukaryotic initiation factor 2; FDR: false discovery rate.

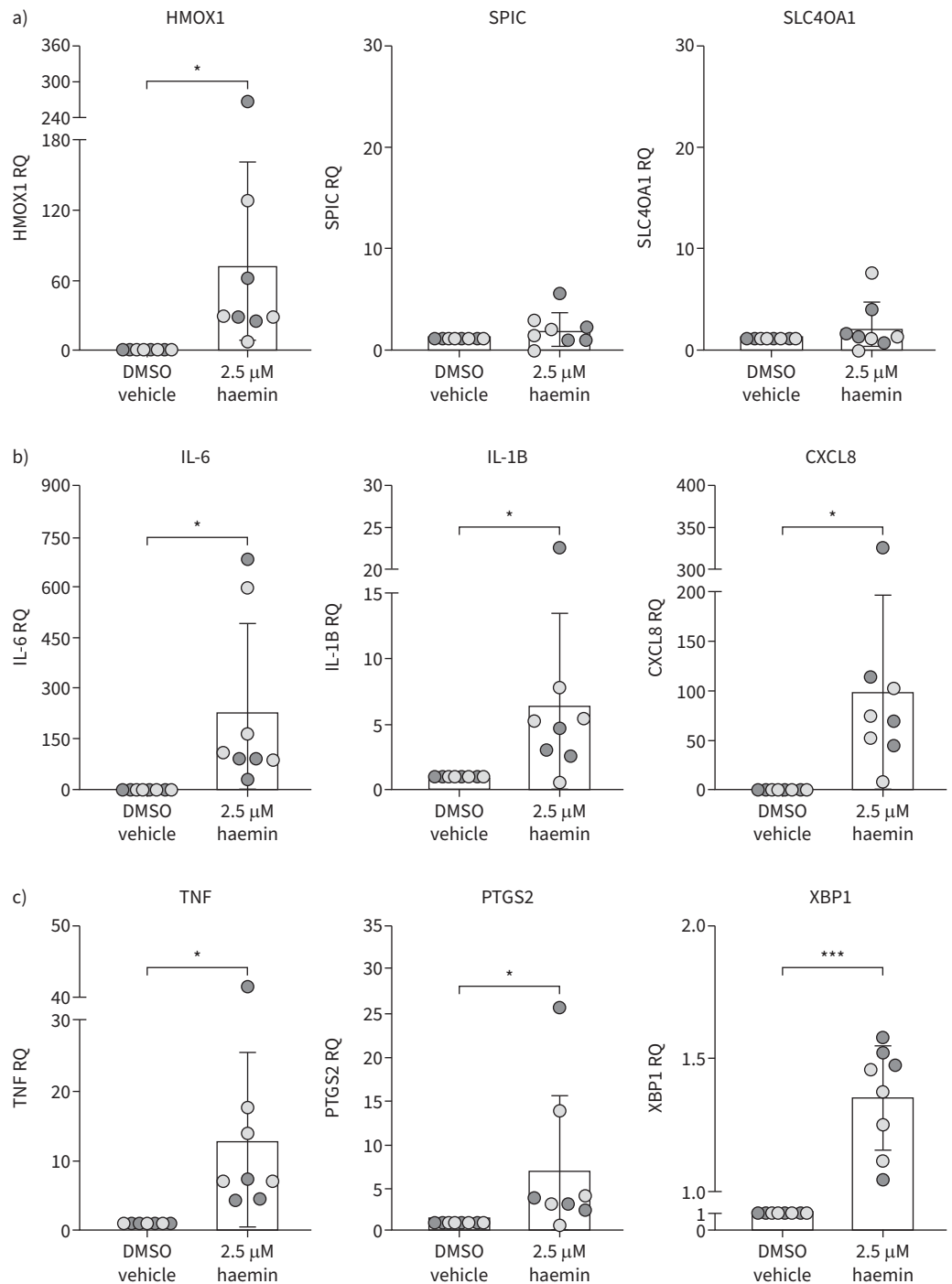


FIGURE 6 *In vitro* activation (2.5 μ M haemin) of iron regulation and M-TPP genes identified by differential gene expression and gene set enrichment analysis analysis of α_1 -antitrypsin deficiency (AATD) bronchoalveolar lavage-obtained alveolar macrophages, as assessed by reverse transcriptase quantitative PCR. **a)** Relative quantities (RQ) of the iron regulatory genes haem oxygenase (HMOX)1 showed significant activation (dimethyl sulfoxide (DMSO) 1.0 ± 0.0 RQ, haemin 72.0 ± 87.5 RQ; $p=0.028$) in AATD and control monocyte-derived macrophages (MDMs), but no activation of the Spi-C transcription factor (SPIC) (DMSO 1.0 ± 0.0 RQ, haemin 2.0 ± 1.7 RQ; $p=0.072$) and SLC40A1 (ferroportin 1) (DMSO 1.0 ± 0.0 RQ, haemin 2.2 ± 2.5 RQ; $p=0.109$) iron efflux regulatory genes by haemin. Relative quantities of **b)** the M-TPP leading edge genes interleukin (IL)-6 (DMSO 1.0 ± 0.0 RQ, haemin 209.5 ± 269.2 RQ; $p=0.032$), IL-1B (DMSO 1.0 ± 0.0 RQ, haemin 6.5 ± 6.9 RQ; $p=0.029$), C-X-C motif chemokine ligand (CXCL)8/IL-8 (DMSO 1.0 ± 0.0 RQ, haemin 98.7 ± 97.7 RQ; $p=0.013$) and **c)** tumour necrosis factor (TNF) (DMSO 1.0 ± 0.0 RQ, haemin 13.0 ± 12.4 RQ; $p=0.032$), prostaglandin-endoperoxide synthase (PTGS)2 (DMSO

1.0±0.0 RQ, haemin 7.2±8.5 RQ; p=0.039) and X-box binding protein (XBP)1 (DMSO 1.0±0.0 RQ, haemin 1.4±0.2 RQ; p=0.0007), all showing significant activation or RNA splicing (XBP1). *: p<0.05; ***: p<0.001 (t-test).

HAADF-STEM imaging data revealed ferritin iron cores either in the cytoplasm or loosely aggregated in autosome-like vesicles in control AlvMacs (figure 4a–c). Ferritin core morphology indicated submaximal iron loading (inset figure 4d) [22]. In AlvMacs from AATD subjects (figure 4e–h), lysosomes were densely packed with iron cores showing maximal loading (figure 4g inset) and lacked the protein cage “halos” (figure 4h). These cores are characterised by a crystalline structure of haematite, as shown (figure 4h inset). Electron microscopy immunogold imaging showed that loss of ferritin protein cages was significantly correlated with increased lysosomal iron content (figure 4i–l). HAADF-STEM quantitative assessment of lysosomal iron accumulation combined with elemental mapping and energy-dispersive X-ray spectroscopy showed that iron was the dominant element in AlvMac lysosomal vesicles (figure 4m–p). Iron-replete lysosomal vesicles were seen in AATD macrophages also containing phagolysosome-type vesicles with nonmetal materials (supplementary figure S1e–h and i–l). Quantitative analysis showed that lysosomal vesicles in tissue sections from AATD subjects contained numbers of ferritin cores orders of magnitude larger relative to the tissue sections from control subjects (supplementary figure S2). Overall, histological, histochemical and electron microscopy assessment showed massive AlvMac iron accumulation consistent with alveolar haemorrhage [23].

RNA sequencing

RNA sequencing pathway analysis in AlvMacs from AATD showed a significant enrichment of pathways related to macrophage innate immune response activation (supplementary figure S3b). This analysis also showed negative enrichment of the canonical pathways “oxidative phosphorylation” and “nucleotide excision repair”, suggesting oxidative stress-induced damage (figure 5a and supplementary figure S3c). AlvMac activation was further explored by gene set enrichment analysis (GSEA) with nine gene sets [18] that, in addition to M1 and M2 [24], identified activation of innate immune activation patterns [18]. GSEA analysis showed positive enrichment of the M-TPP pattern, with negative enrichment of the interferon- γ -activated M1 pattern (figure 5b and supplementary table S1, sheet 1). This suggests that AATD AlvMacs may be activating damage-associated molecular patterns (DAMPs) similar to free haem [10].

In vitro haemin exposure of monocyte-derived macrophages from both AATD2 and control subjects showed results consistent with GSEA findings. Data revealed a significant upregulation of IL-6, IL-1B, CXCL8/IL-8 and TNF cytokine/chemokine genes, as well as PTGS2 and the XBP1 spliced isoform genes (figure 6b, c). These genes are all comprised in the M-TPP upregulated genes (supplementary table S1, sheet 2), as shown by GSEA analysis. In contrast, the M1 genes CXCL9, CXCL10 and CXCL11 were not induced by haemin *in vitro* (supplementary figure S4 and table S1, sheet 3).

MDM exposure to haemin *in vitro* was also used (figure 6a) to assess the expression of genes characterising iron homeostasis. While the HMOX1 gene was upregulated, the iron efflux regulatory genes SPIC and SLC40A1/FPN were not.

Oxidative stress damage assessment

In vitro evaluation of the role of free haem in the generation of oxidative stress, using haemin-stimulated MDM cultures, showed significant ROS production that was not inhibited by AAT, as tested at normal ELF concentration (figure 7a).

Ex vivo assessment of ROS-induced lung tissue damage using 8-OHdG immunohistochemistry demonstrated significantly higher levels of DNA oxidation in AATD lung explants. Relative to controls (figure 7b), AATD explants showed significantly more intense 8-OHdG nuclear staining in alveolar macrophages, interstitial and epithelial cells (figure 7c,d). In particular, AATD epithelial cells showed positive staining in up to 80% of nuclei. In this regard, TEM imaging showed that, relative to controls (figure 7e,f), AATD alveolar epithelial cells had increased numbers of cytoplasmic ferritin cores (figure 7g,h), suggesting a damaging role of iron accumulation in AATD lung epithelial cells, as predicted by previous *in vitro* studies [7].

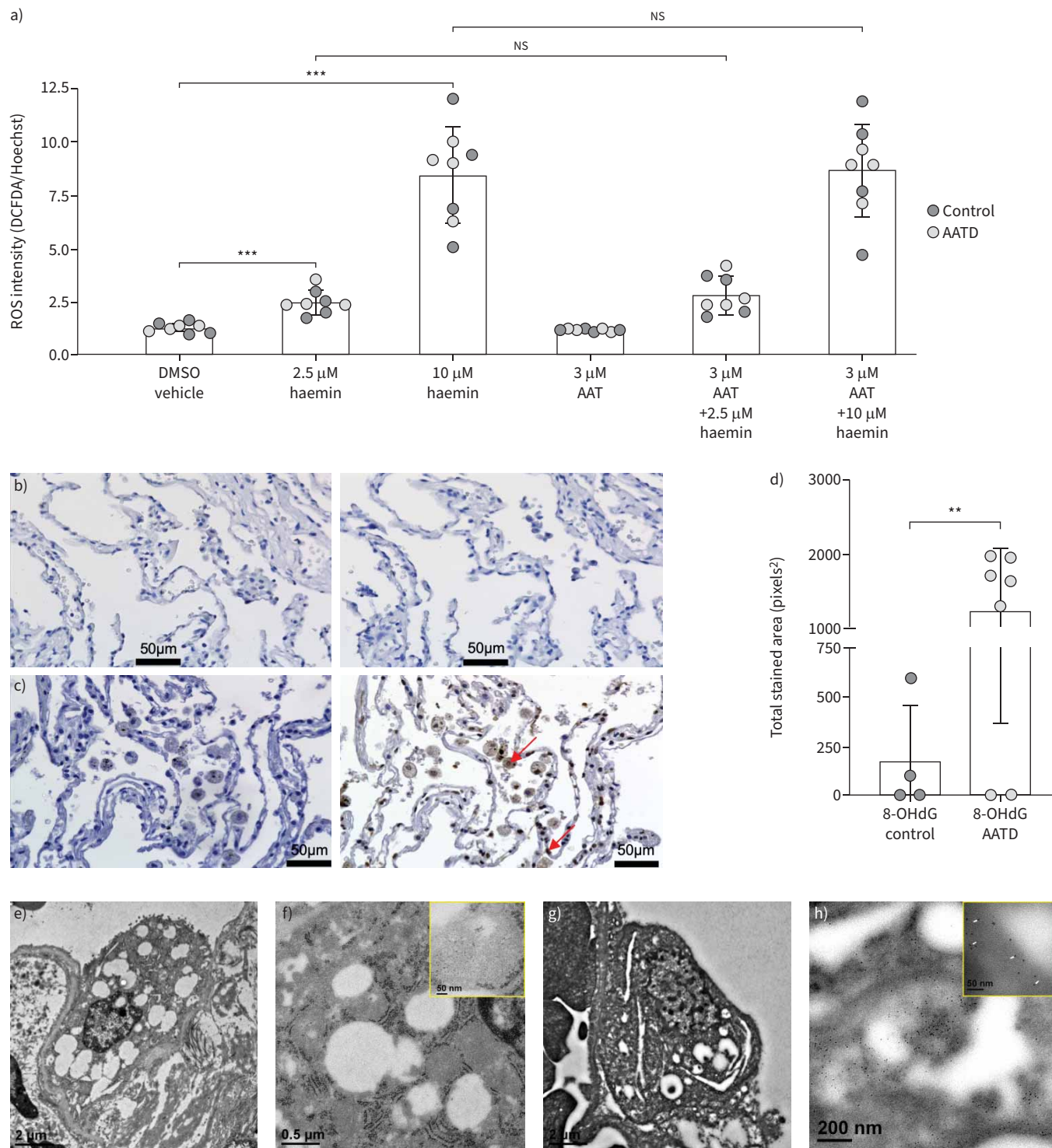


FIGURE 7 a) *In vitro* reactive oxygen species (ROS) generation by α_1 -antitrypsin deficiency (AATD) and control monocyte-derived macrophages (MDMs) induced by 2.5 μ M haemin (dimethyl sulfoxide (DMSO) 1.3 \pm 0.2 dichlorodihydrofluorescein diacetate (DCFDA) fluorescence intensity, 2.5 μ M haemin 2.5 \pm 0.5 intensity; $p=0.0001$) and 10 μ M haemin (DMSO 1.3 \pm 0.2 intensity, 10 μ M haemin 8.5 \pm 2.3 intensity; $p=0.000014$) was significantly higher than vehicle control both in AATD and control. ROS generation by AATD or control MDMs was not inhibited by α_1 -antitrypsin (AAT) at the normal epithelial lining fluid concentration (3 μ M). b) *Ex vivo* assessment of oxidative nuclear damage by 8-hydroxy-2'-deoxyguanosine (8-OHdG) immunohistochemistry in a control lung tissue section. The “no primary” antibody, or control, stain is shown on the left and the 8-OHdG antibody stain on the right image. c) As above, control and 8-OHdG antibody stain of an AATD lung tissue section. The number of 8-OHdG stained nuclei was obtained by subtracting the numbers of brown stained nuclei in primary antibody slides from the number of counterstained (blue) nuclei on the “no primary” slide using ImageJ. Compared to control, numerous epithelial cells and macrophages (arrows) showing 8-OHdG positive nuclei were

seen in AATD. **d**) Compared to control (178.1±282.1 pixels² total stained area), significantly higher numbers of 8-OHdG-positive nuclei are seen in AATD sections (1231.1±866.2 pixels² total stained area, $p=0.009$). ns: nonsignificant. **: $p<0.01$; ***: $p<0.001$ (t-test). **e** and **f**) Bright-field transmission electron microscopy imaging shows a type II epithelial cell **e**) of control tissue, and at higher magnification of the cytoplasm, iron cores are absent (**f**, inset). **g** and **h**) In AATD lung tissue, **g**) a type II epithelial cell shows sparse iron cores in the cytoplasmic reticulum (**h**, inset, arrows).

Discussion

This study provides *ex vivo* evidence for alveolar haemorrhage occurring in subjects with AATD. The results provide evidence of alveolar and interstitial haemorrhage in AATD subjects. The data revealed the elevated concentration of free haem in BAL samples from AATD subjects reflecting recent or actual alveolar bleeding [8, 12]. Additionally, the study shows a massive accumulation of iron in AATD BAL and lung tissue macrophages, a histological marker of “remote” alveolar haemorrhage [9, 23]. Haemopexin can protect against haem toxicity by binding and transporting it to the liver. In AATD fluid, the concentrations of haemopexin, possibly downregulated by Toll-like receptor activation [25], and AAT were too low to scavenge the free haem concentrations [12, 21]. The data show that unopposed free haem, liberated in lung alveoli at levels similar to those found in haemolytic disorders [26], and in the absence of sufficient levels of haemopexin [13], represents a key pro-inflammatory and damaging factor [8, 12].

Consistent with the results of the study showing that haemorrhage corresponded to an elastase dose [27], a significant correlation was observed in this investigation between neutrophil elastase and free haem concentrations measured in the BAL fluids. Neutrophil inflammation can be associated with lung haemorrhage [28]. In cystic fibrosis, where the release of elastase by accumulated neutrophils has been shown to inactivate AAT [29], a study demonstrated abnormal levels of haem and nonencapsulated haemoglobin in BAL fluids. This suggests lower respiratory tract microbleeds [30]. In AATD, the lack of anti-elastase capacity makes neutrophil-released elastase much more damaging, even if neutrophil numbers in the AATD lung are lower than in cystic fibrosis.

Free haem, an inducer of ROS generation and cytokine production [10, 11], can be a key factor in lung injury [8, 12]. Using a set of nine macrophage activation phenotypes [18], we were able to demonstrate upregulation of the expression of the M-TTP macrophage innate immune activation pattern. This pattern is induced by activation of DAMP/pathogen-associated molecular pattern receptors in macrophages [18, 24]. It includes the cytokines TNF, IL-1B and IL-6, associated with the M1 phenotype [31], and IL-8, also induced by neutrophil elastase [32]. As the M-TTP pattern has been shown to be overexpressed by monocytes in sepsis [33], the activation of M-TTP leading-edge genes was replicated in AATD and control MDM haemin-stimulated cultures. This suggests that AATD AlvMacs could be activated by free haem *in vivo*. A model of this process is shown (figure 8).

Lung macrophages, contrary to spleen red pulp macrophages, express an iron-sequestering phenotype [20], that is seen in AATD BAL macrophages using DGE analysis. AATD AlvMacs accumulate iron in lysosomes, as shown by electron microscopy, strongly suggesting alveolar haemorrhage-induced iron sequestration [9, 23, 34]. Increased synthesis of ferritin, the iron carrier protein capable of storing up to 4500 iron atoms [35], protects lung macrophages from oxidative stress in normal, COPD [36] and idiopathic pulmonary haemosiderosis subjects [37]. Contrary to controls, AATD AlvMac iron accumulation is maximal. With a three-fold increase in ferritin, as seen using immunohistochemistry, we found a 1000-fold iron accumulation in AATD. Furthermore, HAADF-STEM showed that while control AlvMac ferritin iron contained ferrihydrite, ferritin iron cores packed in macrophage lysosomes in AATD AlvMacs contained hematite and showed degradation of the ferritin protein cages. Effective ferritin protection against oxidative stress in AATD could thus be challenged.

Consistent with a COPD study using 8-OHdG immunostaining [38], showing more severe damage in AATD-affected than in non-AATD COPD subjects, we found markedly more severe nucleic acid oxidative damage in AATD than in control lung tissues. In addition to AlvMacs, up to 80% of AATD alveolar epithelial cells showed accumulation of iron cores in the endoplasmic reticulum and were affected by oxidative nucleic acid damage. Overall, the findings of increased free haem and iron concentrations in AATD BAL, together with increased iron accumulation and ferritin degradation in lung AlvMacs, are consistent with oxidative stress damage.

In AATD, the loss of AAT serine protease inhibitory capacity has been shown to alter hepcidin regulation of iron homeostasis [39], leading to increased non-haem iron and ferritin blood levels of affected

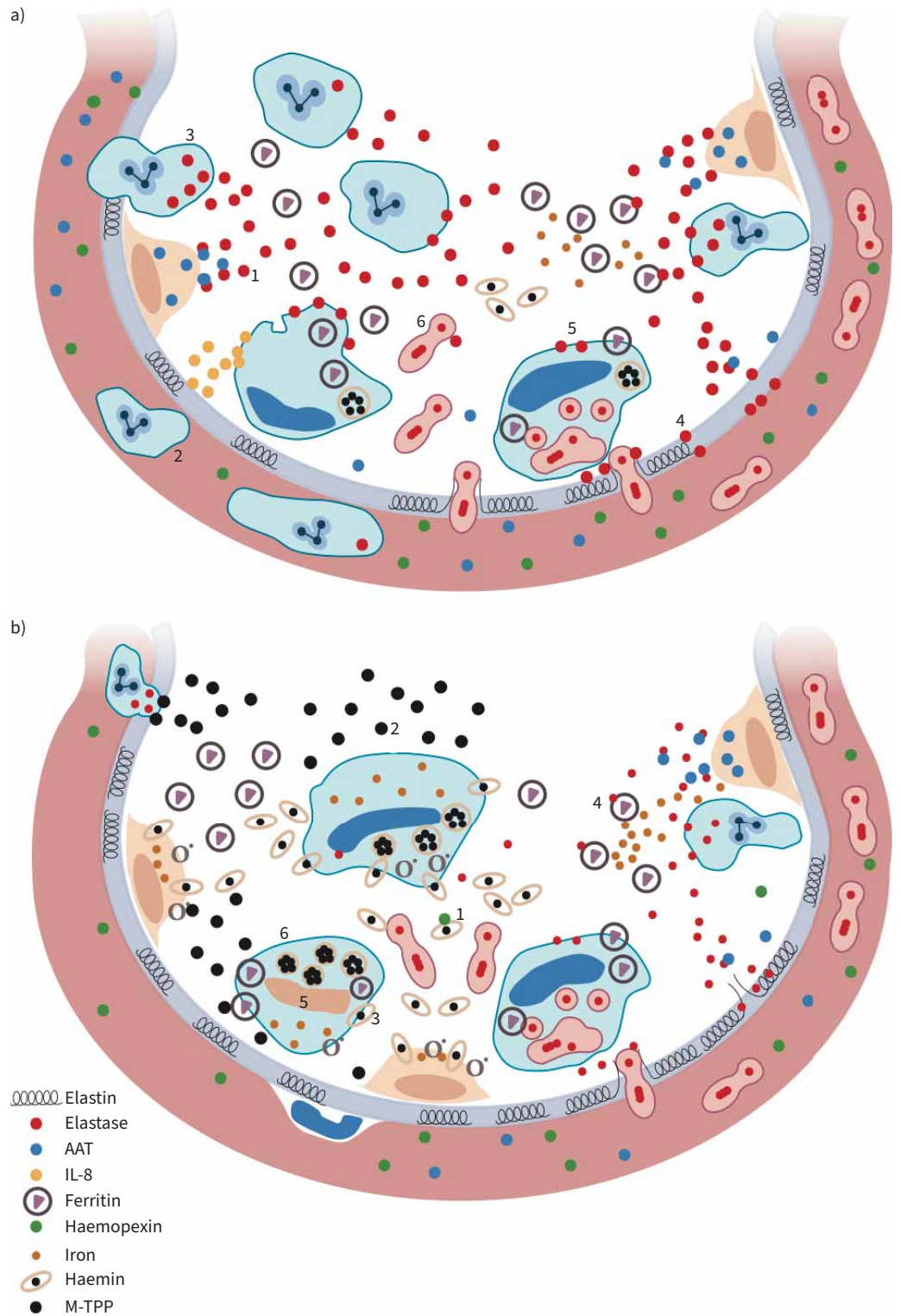


FIGURE 8 a) Haemorrhage. 1) Alveolar macrophage activation by pathogen-associated or damage-associated molecular patterns induces expression of interleukin (IL)-8 and auto-activation of α_1 -antitrypsin (AAT) expression to 2) induce neutrophil chemotaxis with 3) release of AAT-unmatched elastase. 4) Excess elastase causes alveolar membrane damage with red blood cell (RBC) diapedesis into the alveolar spaces. 5) Erythrophagocytosis leads to intracellular accumulation of ferritin and release into the alveolar spaces. 6) RBC lysis leads to haemoglobin and haem release in the alveolar fluid. b) Iron accumulation, inflammation and damage. In the presence of alveolar haemorrhage, 1) the levels of

haemin increase beyond the normal alveolar concentration of haemopexin and 2) activate the M-TPP cytokine response (including IL-8, tumour necrosis factor and IL-6) and 3) oxygen radical production by alveolar macrophages. In the presence of unopposed elastase, 4) alveolar fluid ferritin is digested, with the liberation of high levels of iron. Haemin-induced generation of oxidative stress causes severe nuclear damage in iron-loaded 5) alveolar epithelial cells (brown nuclei) and 6) alveolar macrophages (brown nuclei).

subjects [40]. Most importantly in regard to our study, the lack of AAT antiprotease capacity has been shown to allow degradation of lung extracellular fluid ferritin by unopposed neutrophil elastase. Furthermore, non-haem iron released by degraded ferritin could be imported by alveolar epithelial cells, as seen by BF-TEM imaging in AATD lung tissue, and can increase susceptibility to oxidative stress [7]. Thus, susceptibility of iron-carrying proteins to proteases normally inhibited by AAT could play a critical role in compounding free haem damage, as oxidative damage immunohistochemistry data suggest.

Clearly, there are some limitations to the present study. For example, the numbers of AATD and control lung explants available for histology and electron microscopy, the restricted quantities of lavage fluid, alveolar macrophages and blood cells available from patients with AATD and small numbers of BAL macrophage samples with high-quality RNA. Subsequently, antigenic rather than active neutrophilic elastase was quantified in the lavage fluid and proteases other than neutrophil elastase, which are potentially involved in the genesis of lung disease, were not measured. These same limitations defined the number of end-points measured with regard to 1) the associations of elastase levels with inflammation and iron homeostasis and 2) the potential involvement of components other than neutrophilic elastase and alternative pathways (*e.g.* specific receptors) in the inflammatory response and iron homeostasis could not be examined. In addition, the haem inhibitory capacity of haemopexin and AAT could not be tested *in vitro*. Subsequently, further studies are required to define the role of AAT deficiency in intracellular ferritin degradation and iron accumulation in AATD lung cells.

This notwithstanding, the data presented indicate that the loss of AAT anti-elastase capacity makes AATD subjects susceptible to chronic/recurrent alveolar haemorrhage. The subsequent liberation of free haem in the alveolar spaces may drive accelerated and progressive lung injury as suggested by elastase instillation studies [3].

Provenance: Submitted article, peer reviewed.

Conflict of interest: Y. Xin declares funding for the present work from the National Science Foundation (Cooperative Agreement number DMR-1644779) and the State of Florida. M. Brantly declares funding for the present work from the Alpha-1 Foundation, of which they are Scientific Director. All other authors declare no competing interests.

Support statement: This work was supported by Gatorade Trust through funds distributed by the University of Florida, Department of Medicine (to C. Saltini); the National High Magnetic Field Laboratory (National Science Foundation Cooperative Agreement number DMR-1644779 and the State of Florida) (to Y. Xin); and the Alpha-1 Foundation Professorship (to M. Brantly). Funding information for this article has been deposited with the Crossref Funder Registry.

References

- 1 Greene CM, Marciniak SJ, Teckman J, *et al.* α 1-Antitrypsin deficiency. *Nat Rev Dis Primers* 2016; 2: 16051.
- 2 Brantly ML, Paul LD, Miller BH, *et al.* Clinical features and history of the destructive lung disease associated with alpha-1-antitrypsin deficiency of adults with pulmonary symptoms. *Am Rev Respir Dis* 1988; 138: 327–336.
- 3 Kaplan PD, Kuhn C, Pierce JA. The induction of emphysema with elastase. I. The evolution of the lesion and the influence of serum. *J Lab Clin Med* 1973; 82: 349–356.
- 4 Cosgrove S, Chotirmall SH, Greene CM, *et al.* Pulmonary proteases in the cystic fibrosis lung induce interleukin 8 expression from bronchial epithelial cells *via* a heme/meprin/epidermal growth factor receptor/Toll-like receptor pathway. *J Biol Chem* 2011; 286: 7692–7704.
- 5 Lucey EC, Keane J, Kuang PP, *et al.* Severity of elastase-induced emphysema is decreased in tumor necrosis factor- α and interleukin-1 β receptor-deficient mice. *Lab Invest* 2002; 82: 79–85.
- 6 Ueno M, Maeno T, Nishimura S, *et al.* Alendronate inhalation ameliorates elastase-induced pulmonary emphysema in mice by induction of apoptosis of alveolar macrophages. *Nat Commun* 2015; 6: 6332.

- 7 Fischer BM, Domowicz DA, Zheng S, et al. Neutrophil elastase increases airway epithelial nonheme iron levels. *Clin Transl Sci* 2009; 2: 333–339.
- 8 Shaver CM, Upchurch CP, Janz DR, et al. Cell-free hemoglobin: a novel mediator of acute lung injury. *Am J Physiol Lung Cell Mol Physiol* 2016; 310: L532–L541.
- 9 De Lassece A, Fleury-Feith J, Escudier E, et al. Alveolar hemorrhage. Diagnostic criteria and results in 194 immunocompromised hosts. *Am J Respir Crit Care Med* 1995; 151: 157–163.
- 10 Dutra FF, Bozza MT. Heme on innate immunity and inflammation. *Front Pharmacol* 2014; 5: 115.
- 11 Figueiredo RT, Fernandez PL, Mourao-Sa DS, et al. Characterization of heme as activator of Toll-like receptor 4. *J Biol Chem* 2007; 282: 20221–9.
- 12 Larsen R, Gozzelino R, Jeney V, et al. A central role for free heme in the pathogenesis of severe sepsis. *Sci Transl Med* 2010; 2: 51ra71.
- 13 Vinchi F, Costa da Silva M, Ingoglia G, et al. Hemopexin therapy reverts heme-induced proinflammatory phenotypic switching of macrophages in a mouse model of sickle cell disease. *Blood* 2016; 127: 473–486.
- 14 Sindrilaru A, Peters T, Wieschalka S, et al. An unrestrained proinflammatory M1 macrophage population induced by iron impairs wound healing in humans and mice. *J Clin Invest* 2011; 121: 985–997.
- 15 Zhou Y, Que KT, Zhang Z, et al. Iron overloaded polarizes macrophage to proinflammation phenotype through ROS/acetyl-p53 pathway. *Cancer Med* 2018; 7: 4012–4022.
- 16 Brantly M, Stocks J, Rouhani F, et al. Inhaled alpha-1-antitrypsin restores lower respiratory tract protease–anti-protease homeostasis and reduces inflammation in alpha-1 antitrypsin deficient individuals: a phase 2 clinical study using inhaled kamada-api. *Am J Respir Crit Care Med* 2017; 195: A7677.
- 17 Rennard SI, Basset G, Lecossier D, et al. Estimation of volume of epithelial lining fluid recovered by lavage using urea as marker of dilution. *J Appl Physiol* 1986; 60: 532–538.
- 18 Xue J, Schmidt SV, Sander J, et al. Transcriptome-based network analysis reveals a spectrum model of human macrophage activation. *Immunity* 2014; 40: 274–288.
- 19 Krotova K, Marek GW, Wang RL, et al. Alpha-1 antitrypsin-deficient macrophages have increased matriptase-mediated proteolytic activity. *Am J Respir Cell Mol Biol* 2017; 57: 238–247.
- 20 Kohyama M, Ise W, Edelson BT, et al. Role for Spi-C in the development of red pulp macrophages and splenic iron homeostasis. *Nature* 2009; 457: 318–321.
- 21 Karnaukhova E, Krupnikova SS, Rajabi M, et al. Heme binding to human alpha-1 proteinase inhibitor. *Biochim Biophys Acta* 2012; 1820: 2020–2029.
- 22 Jian N, Dowle M, Horniblow RD, et al. Morphology of the ferritin iron core by aberration corrected scanning transmission electron microscopy. *Nanotechnology* 2016; 27: 46LT02.
- 23 Brambilla CG, Brambilla EM, Stoebner P, et al. Idiopathic pulmonary hemorrhage. Ultrastructural and mineralogic study. *Chest* 1982; 81: 120–123.
- 24 Murray PJ, Allen JE, Biswas SK, et al. Macrophage activation and polarization: nomenclature and experimental guidelines. *Immunity* 2014; 41: 14–20.
- 25 Yang N, Zhang L, Tian D, et al. Tanshinone increases hemopexin expression in lung cells and macrophages to protect against cigarette smoke-induced COPD and enhance antiviral responses. *Cell Cycle* 2023; 22: 645–665.
- 26 Plewes K, Kingston HWF, Ghose A, et al. Cell-free hemoglobin mediated oxidative stress is associated with acute kidney injury and renal replacement therapy in severe falciparum malaria: an observational study. *BMC Infect Dis* 2017; 17: 313.
- 27 Limjunyawong N, Craig JM, Lagassé HA, et al. Experimental progressive emphysema in BALB/cJ mice as a model for chronic alveolar destruction in humans. *Am J Physiol Lung Cell Mol Physiol* 2015; 309: L662–L676.
- 28 Kanaoka K, Minami S, Ihara S, et al. High neutrophils and low lymphocytes percentages in bronchoalveolar lavage fluid are prognostic factors of higher in-hospital mortality in diffuse alveolar hemorrhage. *BMC Pulm Med* 2021; 21: 288.
- 29 Meyer KC, Lewandoski JR, Zimmerman JJ, et al. Human neutrophil elastase and elastase/alpha 1-antiprotease complex in cystic fibrosis. Comparison with interstitial lung disease and evaluation of the effect of intravenously administered antibiotic therapy. *Am Rev Respir Dis* 1991; 144: 580–585.
- 30 Ghio AJ, Roggli VL, Soukup JM, et al. Iron accumulates in the lavage and explanted lungs of cystic fibrosis patients. *J Cyst Fibros* 2013; 12: 390–398.
- 31 Mantovani A, Sica A, Sozzani S, et al. The chemokine system in diverse forms of macrophage activation and polarization. *Trends Immunol* 2004; 25: 677–686.
- 32 Krotova K, Khodayari N, Oshins R, et al. Neutrophil elastase promotes macrophage cell adhesion and cytokine production through the integrin-Src kinases pathway. *Sci Rep* 2020; 10: 15874.
- 33 Liepelt A, Hohlstein P, Gussen, H, et al. Differential gene expression in circulating CD14⁺ monocytes indicates the prognosis of critically ill patients with sepsis. *J Clin Med* 2020; 9: 127.
- 34 Möller W, Barth W, Kohlhäufel M, et al. Human alveolar long-term clearance of ferromagnetic iron oxide microparticles in healthy and diseased subjects. *Exp Lung Res* 2001; 27: 547–568.
- 35 Gupta R, Alamrani NA, Greenway GM, et al. Method for determining average iron content of ferritin by measuring its optical dispersion. *Anal Chem* 2019; 91: 7366–7372.

- 36 Olakanmi O, McGowan SE, Hayek MB, *et al.* Iron sequestration by macrophages decreases the potential for extracellular hydroxyl radical formation. *J Clin Invest* 1993; 91: 889–899.
- 37 Persson HL, Vainikka LK, Eriksson HB, *et al.* Lane–Hamilton syndrome: ferritin protects lung macrophages against iron and oxidation. *Chest* 2011; 139: 361–367.
- 38 Deslee G, Woods JC, Moore C, *et al.* Oxidative damage to nucleic acids in severe emphysema. *Chest* 2009; 135: 965–974.
- 39 Schaefer B, Haschka D, Finkenstedt A, *et al.* Impaired hepcidin expression in alpha-1-antitrypsin deficiency associated with iron overload and progressive liver disease. *Hum Mol Genet* 2015; 24: 6254–6263.
- 40 Ghio AJ, Soukup JM, Richards JH, *et al.* Deficiency of α -1-antitrypsin influences systemic iron homeostasis. *Int J Chron Obstruct Pulmon Dis* 2013; 8: 45–51.